Dynamically Stable Bipedal Robotic Walking with NAO via Human-Inspired Hybrid Zero Dynamics

Aaron D. Ames
Department of Mechanical Engineering,
Texas A&M University,
College Station, TX 77843
aames@tamu.edu

Eric A. Cousineau
Department of Mechanical Engineering,
Texas A&M University,
College Station, TX 77843
eacousineau@tamu.edu

Matthew J. Powell
Department of Mechanical Engineering,
Texas A&M University,
College Station, TX 77843
mjpowell@tamu.edu

ABSTRACT

This paper demonstrates the process of utilizing human locomotion data to formally design controllers that yield provably stable robotic walking and experimentally realizing these formal methods to achieve dynamically stable bipedal robotic walking on the NAO robot. Beginning with walking data, outputs—or functions of the kinematics—are determined that result in a low-dimensional representation of human locomotion. These same outputs can be considered on a robot, and *human-inspired control* is used to drive the outputs of the robot to the outputs of the human. An optimization problem is presented that determines the parameters of this controller that provide the best fit of the human data while simultaneously ensuring *partial hybrid zero dynamics*. The main formal result of this paper is a proof that these same parameters result in a stable hybrid periodic orbit with a fixed point that can be computed in closed form. Thus, starting with only human data we obtain a stable walking gait for the bipedal robot model. These formal results are validated through experimentation: implementing the stable walking found in simulation on NAO results in dynamically stable robotic walking that shows excellent agreement with the simulated behavior from which it was derived.

Categories and Subject Descriptors

J.2 [**Physical Sciences and Engineering**]: [engineering, mathematics and statistics]; G.1.6 [**Numerical Analysis**]: Optimization—*constrained optimization*

General Terms

Theory, Algorithms, Experimentation

Keywords

hybrid systems, bipedal robotic walking, nonlinear dynamics and control, human-data based optimization

HSCC'12, April 17–19, 2012, Beijing, China.

1. INTRODUCTION

Aldebaran's commercially available NAO robot ships with a pre-packaged walking algorithm called the "Stable and Omnidirectional Walk"; this algorithm implements a pattern generation technique which utilizes the Zero-Moment Point (ZMP)[1, 11]. Indeed, the ZMP is a popular choice of controller in the robotic walking community [20]. Other interesting approaches to the bipedal robotic walking problem have surfaced in the field's long history, including passive walking and controlled symmetries [6, 18], capture point [14], geometric reduction [4, 8, 17] and hybrid nonlinear feedback control [7, 22], to name a only a few. Of the current research in the field, the philosophy toward walking taken in this paper can be best related to the spring-loaded inverted pendulum [9], or SLIP model, due to its methodology of representing locomotion by a simple "virtual" system. Common to these approaches is the application of control theory and understanding of dynamics to achieve and implement impressive walking algorithms and motion generators; however, there exists a significant disparity between the walking achieved with these methods and the actual, dynamically stable walking displayed by humans.

This paper presents a distinctively different approach to the bipedal robotic walking control design problem: look to human walking data to motivate the *formal design* of controllers that achieve provably stable robotic walking. The main idea is that regardless of the complexity present in human walking—hundreds of degrees of freedom coupled with highly nonlinear dynamics and forcing due to the 57 muscles employed during human walking [15]—the essential information needed to understand walking is encoded by a simple class of functions. In other words, taking the control theorist approach to understanding a complex and unknown system, we view the human walking system as a "black box," where the "input" to the system is a specific walking behavior, and we seek "outputs" of this system that characterize these walking behaviors. These outputs

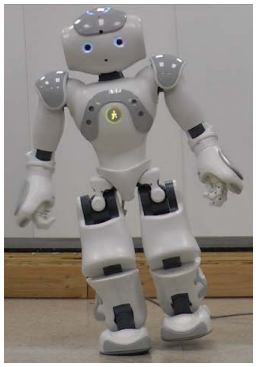

Figure 1: Experimental demonstration of NAO displaying dynamically stable walking.

can then be utilized in the design of robotic controllers—the outputs of the robot can be driven to the outputs of the human, resulting in "human-like" robotic walking.

Given human walking as the motivation for achieving robotic walking, this paper begins by looking at human walking data, i.e., angles over time, achieved through motion capture of subjects walking on flat ground at a "natural" pace. Indeed, work with human data to construct low dimensional representations of human walking has been performed [19] by fitting human data with Bézier curves; however, the work presented here suggests insight beyond achieving "best fits" to data. By studying human data, we discover a collection of outputs that appear to characterize human walking—they are mutually exclusive, thus providing a low dimensional representation of the system's behavior. Moreover, we find that these *human outputs*, as computed from the data, appear to be described by a very simple function: the time solution to a linear spring-mass-damper system. We term this function the *canonical human walking function*, and verify that in fact this function describes the human data by showing that it can be fit to the human data with a remarkably high correlation coefficient. Utilizing the human outputs and their time-based representation given by the canonical walking functions, we construct a *human-inspired* controller that drives the outputs of the robot to the outputs of the human as represented by the canonical walking functions.

The main result of this paper is a formal method for determining the parameters of the human-inspired controller that provably results in stable robotic walking for a planar biped that is as "human-like" as possible. In particular, we introduce an optimization problem where the cost is the least squares fit of the outputs of the robot to the human output data subject to constraints that ensure *partial hybrid zero dynamics* [3], i.e., constraints that ensure that the zero dynamics surface associated with the relative degree 2 output functions is invariant through impact. This invariance allows us to characterize the behavior of the hybrid system modeling a bipedal robot (which is 10 dimensional for the model considered) through a 2-dimensional hybrid system. Utilizing this reduced dimensional representation, we are able to prove the main result of this paper: the parameters that solve the partial hybrid zero dynamics optimization problem imply the existence of an exponentially stable hybrid periodic orbit, i.e., the existence of a stable walking gait; moreover, the fixed point of the Poincaré map associated with this periodic orbit can be explicitly computed from these parameters. In other words, using only the human data, we are able to automatically generate parameters for the human inspired controller that imply the existence of a stable walking gait, and we can explicitly compute the initial condition to this walking gait from these parameters.

To supplement the main theoretical developments of this paper, we experimentally apply them to Aldebaran's NAO robot [1]. By considering the 2D hybrid system model of this robot, we use the main results of the paper to obtain stable robotic walking in simulation using only human data. The trajectories obtained through simulation are implemented on NAO, together with a simple online lateral stability feedback controller. The end result is dynamically stable walking on NAO that is markedly more human-like than pre-existing walking achieved with NAO (as evidenced by the walking itself and the comparison of this walking with the pre-existing NAO walking, both of which can be seen at [2]). Thus we have successfully utilized human data to formally achieve "human-like" robotic walking and demonstrated these results experimentally.

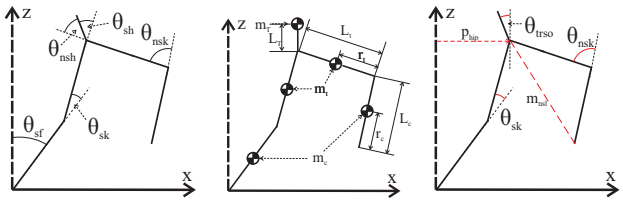

(a) Configuration (b) Mass/length (c) Constraints

Figure 2: The modeled robot's configuration, mass & length distribution, and virtual constraints (outputs).

2. HUMAN WALKING DATA

As the ultimate goal of this work is to develop a control scheme which yields stable human-like robotic walking, we turn to the human locomotion data for insight in the design process. Examination of human walking data reveals that certain outputs of the human locomotion system can be represented as second order linear system responses. This section, therefore, introduces these outputs and shows that the human data for these outputs can be accurately fit by the time-solution to a linear mass-spring-damper system.

Human Walking Experiment. The goal of this experiment was to track the evolution of the spatial positions of specific points on the human body during walking on flat ground—this collection of position data forms the raw kinematic outputs of human walking. For each trial, LED sensors were fixed to a test subject in key locations, such as the joints, along the lower body—as the test subject walked forward, the spatial position of each LED sensors was measured at 480 Hz. A total of 11 trials per test subject and a total of 9 test subjects were considered. For purposes of this paper, the mean data from all 9 subjects are considered; see [5] for more information regarding the walking experiments.

Human Outputs. Common in the bipedal robotic walking literature is the employment of nonlinear feedback linearization [16, 22]. In this method, "virtual outputs" are specified which, upon successful application of feedback linearization control, constrain the motion of a controlled robot. These virtual outputs are functions of state, and thus are independent of the robot's actuator dynamics. Furthermore, the same outputs can be computed from human walking data — the result is a direct kinematic relationship between robot and human walking, despite the morphological and dynamical differences in the two systems. With this in mind, we consider the following virtual output functions (see Fig. 2):

1. The linearization of the x-position of the hip, p_{hip}, given by:
$$\delta p_{\text{hip}}(\theta) = L_c(-\theta_{sf}) + L_t(-\theta_{sf} - \theta_{sk}) \qquad (1)$$
with L_c and L_t the length of the calf and thigh.

2. The linearization of the slope of the non-stance leg m_{nsl}, (the tangent of the angle between the z-axis and the line on the non-stance leg connecting the ankle and

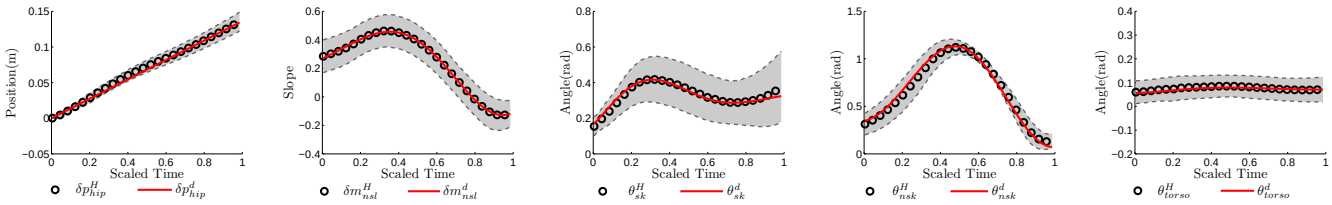

(a) δp_{hip} (b) δm_{nsl} (c) θ_{sk} (d) θ_{nsk} (e) θ_{tor}

Figure 3: The mean human output data for the nine subjects, computed with the parameters for NAO, with error bands showing one standard deviation from the mean, and the canonical walking function fits.

hip), given by:

$$\delta m_{nsl}(\theta) = -\theta_{sf} - \theta_{sk} - \theta_{sh} - \theta_{nsh} + \frac{L_c}{L_c + L_t}\theta_{nsk}. \tag{2}$$

3. The angle of the stance knee, θ_{sk},
4. The angle of the non-stance knee, θ_{nsk},
5. The angle of the torso from vertical,

$$\theta_{tor}(\theta) = \theta_{sf} + \theta_{sk} + \theta_{sh}. \tag{3}$$

These outputs, shown in Fig. 3, were computed from the experimental human walking data which was scaled to the robot by computing $\delta p_{\text{hip}}(\theta)$ and $\delta m_{nsl}(\theta)$ using the NAO's length distribution. This figure also shows the mean of each output computed from the data from nine subjects and error bands showing one standard deviation from this mean. Note that the motivation for considering the linearization of the position of the hip and the non-stance slope (rather than their original nonlinear formulations, as was considered in [3]) will be seen later in the paper—it allows for a simple representation of the partial hybrid zero dynamics.

Human Walking Functions. Visual inspection of the outputs as computed from the human data for the three subjects (see Fig. 3) shows that all of the human outputs appear to be described by two simple functions. In particular, the linearized position of the hip appears to be essentially a linear function of time:

$$\delta p^d_{\text{hip}}(t, v) = v_{hip} t. \tag{4}$$

The remaining human outputs, δm_{nsl}, θ_{sk}, θ_{nsk}, θ_{tor} appear to be described by the solution to a linear mass-spring-damper system. With this in mind, define the *canonical human walking function* as:

$$y_H(t, \alpha) = e^{-\alpha_4 t}(\alpha_1 \cos(\alpha_2 t) + \alpha_3 \sin(\alpha_2 t)) + \alpha_5. \tag{5}$$

This function can be related to the more standard form of the time solution of a mass-spring-damper system by noting that $\alpha_1 = c_0$, $\alpha_2 = \omega_d$, $\alpha_3 = c_1$, $\alpha_4 = \zeta\omega_n$ and $\alpha_5 = g$, where ζ is the damping ratio, ω_n is the natural frequency, $\omega_d = \omega_n\sqrt{1-\zeta^2}$ is the damped natural frequency, c_0 and c_1 are determined by the initial conditions of the system, and g is a gravity related constant. In particular, with (5), for the 4 remaining human outputs, we write:

$$\begin{aligned} m^d_{nsl}(t, \alpha_{nsl}) &= y_H(t, \alpha_{nsl}), & \theta^d_{tor}(t, \alpha_{nsl}) &= y_H(t, \alpha_{tor}), \\ \theta^d_{sk}(t, \alpha_{sk}) &= y_H(t, \alpha_{sk}), & \theta^d_{nsk}(t, \alpha_{nsk}) &= y_H(t, \alpha_{nsk}), \end{aligned} \tag{6}$$

where, e.g., $\alpha_{nsl} = (\alpha_{nsl,1}, \alpha_{nsl,2}, \alpha_{nsl,3}, \alpha_{nsl,4}, \alpha_{nsl,5})$ in (5). The parameters of all of the outputs can be combined to yield a single vector: $\alpha = (v_{\text{hip}}, \alpha_{nsl}, \alpha_{nsk}, \alpha_{sk}, \alpha_{tor}) \in \mathbb{R}^{21}$. If it can be verified that these functions accurately fit the mean human output data, then it can be concluded that humans appear to act like linear spring-mass-damper systems for the chosen outputs.

Human-Data-Based Cost Function. The goal is to show that the human walking functions accurately describe the human data. This will be achieved by simply fitting (5) to the human walking data to achieve a least squares fit. From the mean human walking data, we obtain discrete times, $t^H[k]$, and discrete values for the output functions: $\delta p^H_{\text{hip}}[k]$, $\delta m^H_{nsl}[k]$, $\theta^H_{sk}[k]$, $\theta^H_{nsk}[k]$, and $\theta^H_{tor}[k]$ where here $k \in \{1, \ldots, K\} \subset \mathbb{N}$ with K the number of data points. Represent the mean human output data by $y^H_i[k]$ and the canonical walking functions by $y^d_i(t, \alpha_i)$ for $i \in \text{Output} = \{hip, msl, sk, nsk, tor\}$; for example, $y^H_{msl}[k] = \delta m^H_{nsl}[k]$ and $y^d_{msl}(t, \alpha_{msl}) = \delta m^d_{nsl}(t, \alpha_{nsl})$. Define the following human-data-based cost function:

$$\text{Cost}_{\text{HD}}(\alpha) = \sum_{k=1}^{K} \sum_{i \in \text{Output}} \left(y^H_i[k] - y^d_i(t^H[k], \alpha_i) \right)^2 \tag{7}$$

which is simply the sum of squared residuals. To determine the parameters for the human walking functions, we need only solve the optimization problem:

$$\alpha^* = \underset{\alpha \in \mathbb{R}^{21}}{\text{argmin}} \ \text{Cost}_{\text{HD}}(\alpha) \tag{8}$$

which yields the least squares fit of the mean human output data with the canonical walking functions. The parameters given by solving this optimization problem are stated in Table 1. The correlations, as given in the same table, show that the fitted walking functions very closely model the human output data, i.e., the chosen human walking functions appear to be, in fact, canonical. Indeed, the coefficients of correlation are all very high, ranging from 0.8767 to 0.9997. The accuracy of the fits can be seen in Fig. 3.

3. BIPEDAL ROBOT MODEL (NAO)

Bipedal walking robots naturally display continuous and discrete behavior throughout the course of a step—the continuous behavior occurs when the leg swings forward and the discrete behavior occurs when the foot strikes the ground. It is, therefore, natural to model robots of this form by hybrid systems [5, 17] (also referred to as systems with impulsive effects or systems with impulse effects [7, 8]). This

$y_{H,2} = e^{-\alpha_4 t}(\alpha_1 \cos(\alpha_2 t) + \alpha_3 \sin(\alpha_2 t)) + \alpha_5$							
Fun.	v_{hip}	α_1	α_2	α_3	α_4	α_5	Cor.
δp_{hip}	0.2288	*	*	*	*	*	0.9984
δm_{nsl}	*	-0.0065	8.9157	0.1162	-2.2638	0.2750	0.9997
θ_{sk}	*	-0.1600	12.4473	0.0980	3.6061	0.3240	0.9751
θ_{nsk}	*	-0.3322	-10.2618	-0.1109	-0.9345	0.6772	0.9948
θ_{tor}	*	-0.0166	10.4416	-0.0033	3.2976	0.0729	0.8767

Table 1: Parameter values and correlation coefficients of the canonical human walking functions obtained from optimization about the mean human data and NAO robot model.

section introduces the basic formalisms of hybrid systems along with the specific hybrid model obtained for the robot that is considered in this paper: NAO, as shown in Fig. 1. It is important to note that the model of NAO used in this work is the 2D, planar model with point feet. Analysis of the 3D and finite foot models is a topic of future work.

Hybrid Systems. A (simple) *hybrid control system* is a tuple,

$$\mathscr{HC} = (\mathcal{D}, U, S, \Delta, f, g),$$

where $\mathcal{D}$ is the *domain* with $\mathcal{D} \subseteq R^n$ a smooth submanifold of the state space $\mathbb{R}^n$, $U \subseteq \mathbb{R}^m$ is the set of admissible controls, $S \subset \mathcal{D}$ is a proper subset of $\mathcal{D}$ called the *guard* or *switching surface*, $\Delta : S \to \mathcal{D}$ is a smooth map called the *reset map*, and (f, g) is a *control system* on $\mathcal{D}$, i.e., in coordinates: $\dot{x} = f(x) + g(x)u$. A *hybrid system* is a hybrid control system with $U = \emptyset$, e.g., any applicable feedback controllers have been applied, making the system closed-loop. In this case,

$$\mathscr{H} = (\mathcal{D}, S, \Delta, f),$$

where f is a *dynamical system* on $\mathcal{D} \subseteq \mathbb{R}^n$, i.e., $\dot{x} = f(x)$.

Periodic Orbits. Stable bipedal robotic walking corresponds to stable periodic orbits in hybrid systems. For simplicity, we consider periodic orbits of hybrid systems with fixed points on the guard (for more general definitions, see [8, 21]). Let $\varphi(t, x_0)$ be the solution to $\dot{x} = f(x)$ with initial condition $x_0 \in \mathcal{D}$. For $x* \in S$, we say that φ is *periodic* with period $T > 0$ if $\varphi(T, \Delta(x*)) = x*$. A set $\mathcal{O}$ is a *periodic orbit* with *fixed point* x^* if $\mathcal{O} = \{\varphi(t, \Delta(x^*)) : 0 \leq t \leq T\}$ for a periodic solution φ. Associated with a periodic orbit is a Poincaré map [21]; specifically, taking S to be the Poincaré section, one obtains the Poincaré map $P : S \to S$ which is a partial function:

$$P(x) = \varphi(T_I(x), \Delta(x)),$$

where T_I is the *time-to-impact function* [22]. As with smooth dynamical systems, the stability of the Poincaré map determines the stability of the periodic orbit $\mathcal{O}$. In particular, the Poincaré map is (locally) exponentially stable (as a discrete time system $x_{k+1} = P(x_k)$) at the fixed point x^* if and only if the periodic orbit $\mathcal{O}$ is (locally) exponentially stable [12]. Although it is not possible to analytically compute the Poincaré map, it is possible to numerically compute its Jacobian. Thus, if the eigenvalues of the Jacobian have magnitude less than one, the stability of the periodic orbit $\mathcal{O}$ has been numerically verified.

NAO Hybrid Model. Utilizing the mass and inertia properties of the NAO robot provided in the specifications sheet [1], we can formally model this robot as a hybrid control system:

$$\mathscr{HC}_R = (\mathcal{D}_R, U_R, S_R, \Delta_R, f_R, g_R). \tag{9}$$

The method used to construct the individual elements of this hybrid system will now be discussed.

Continuous Dynamics: The configuration space of the robot $\mathcal{Q}_R$ is given in coordinates by:

$$\theta = (\theta_{sf}, \theta_{sk}, \theta_{sh}, \theta_{nsh}, \theta_{nsk})^T,$$

where, as illustrated in Fig. 2, θ_{sf} is the angle of the stance foot, θ_{sk} is the angle of the stance knee, θ_{sh} is the angle of the torso with the stance thigh, θ_{nsh} is the angle of the non-stance thigh with the torso, and θ_{nsk} is the angle of the non-stance (or swing) knee. Calculating the mass and inertia properties of each link of the robot using the specifications of the robot allows for the construction of the Lagrangian:

$$\mathcal{L}_R(\theta, \dot{\theta}) = \frac{1}{2}\dot{\theta}^T D(\theta)\dot{\theta} - V(\theta). \tag{10}$$

Explicitly, this is done symbolically through the method of exponential twists (see [13]). The Euler-Lagrange equations yield the equations of motion of the form:

$$D(\theta)\ddot{\theta} + H(\theta, \dot{\theta}) = B(\theta)u.$$

Converting the equations of motion to a first order ODE yields the affine control system (f_R, g_R):

$$f_R(\theta, \dot{\theta}) = \begin{bmatrix} \dot{\theta} \\ -D^{-1}(\theta)H(\theta, \dot{\theta}) \end{bmatrix}, \quad g_R(\theta) = \begin{bmatrix} \mathbf{0} \\ D^{-1}(\theta)B(\theta) \end{bmatrix},$$

with $U_R = \mathbb{R}^5$ and $B(\theta) \in \mathbb{R}^{5\times 5}$.

Domain and Guard: The domain specifies the allowable configuration of the system as specified by a unilateral constraint function h_R; for the biped considered in this paper, this function specifies that the non-stance foot must be above the ground, i.e., h_R is the height of the non-stance foot. In particular, the domain $\mathcal{D}_R$ is given by:

$$\mathcal{D}_R = \left\{(\theta, \dot{\theta}) \in T\mathcal{Q}_R : h_R(\theta) \geq 0\right\}.$$

The guard is just the boundary of the domain with the additional assumption that the unilateral constraint is decreasing:

$$S_R = \left\{(\theta, \dot{\theta}) \in T\mathcal{Q}_R : h_R(\theta) = 0 \text{ and } dh_R(\theta)\dot{\theta} < 0\right\},$$

where $dh_R(\theta)$ is the Jacobian of h_R at θ.

Discrete Dynamics. The discrete dynamics of the robot determine how the velocities of the robot change when the foot impacts the ground, while simultaneously switching the "stance" and "non-stance" legs. In particular, the reset map Δ_R is given by:

$$\Delta_R : S_R \to \mathcal{D}_R, \qquad \Delta_R(\theta, \dot{\theta}) = \begin{bmatrix} \Delta_\theta \theta \\ \Delta_{\dot{\theta}}(\theta)\dot{\theta} \end{bmatrix}, \tag{11}$$

where Δ_θ is the relabeling matrix which switches the stance and non-stance leg at impact (by appropriately changing the angles). Here, $\Delta_{\dot{\theta}}$ determines the change in velocity due to impact; we forgo the detailed discussion on its computation, but detailed descriptions can be found in [10], [8] and [3]. In particular, it is computed by considering extended coordinates that include the position of the stance foot and employing a perfectly plastic impact law that results in the

pre-impact non-stance foot being fixed post-impact, wherein it becomes the stance foot.

4. HUMAN-INSPIRED CONTROL

In this section, we construct a human-inspired controller that drives the outputs of the robot to the outputs of the human (as represented by canonical walking functions). Moreover, we render this control law autonomous through a parameterization of time based upon the position of the hip. The end result is a feedback control that is used to obtain stable bipedal robotic walking.

Parameterization of Time. Attracted by the robustness of *autonomous* control, we introduce a state-based parameterization of time in our system; this is a common practice [23, 22], except that in this case we pick a parameterization as motivated by human data. Examination of human data reveals that the (linearized) forward position of the hip evolves in an approximately linear manner with respect to time, that is $\delta p_{hip}(t, v_{hip}) \approx v_{hip} t$, where p_{hip} denotes the forward position of the hip and v_{hip} denotes the forward velocity of the hip. Taking advantage of this observation, the following parameterization of time is formed:

$$\tau(\theta) = \frac{\delta p^R_{\text{hip}}(\theta) - \delta p^R_{\text{hip}}(\theta^+)}{v_{\text{hip}}}. \tag{12}$$

where $\delta p^R_{\text{hip}}(\theta^+)$ is the (linearized) forward position of the robot's hip at the beginning of the current step, and v_{hip} is the forward velocity of the hip (which is just an element of the vector of parameters α).

Output Functions. Based upon the human outputs and their time-based representation given by the canonical walking functions, we define relative degree 1 and (vector) relative 2 outputs for the robot based upon our desire for the robot to have the same output behavior as the human. (Note that it will not be formally verified that these are, in fact relative degree 1 and 2 outputs until the decoupling matrix is introduced; see [16] for a formal definition.)

With the goal of controlling the velocity of the robot, we define the relative degree 1 output from the actual velocity of the hip and the desired velocity of the hip:

$$y_{a,1}(\theta, \dot\theta) = \delta \dot p^R_{\text{hip}}(\theta, \dot\theta) = d\delta p^R_{\text{hip}}(\theta)\dot\theta, \qquad y_{d,1} = v_{\text{hip}}. \tag{13}$$

where $\delta p^R_{\text{hip}}(\theta)$ is given in (1). Since $y_{a,1}$ is the output of a mechanical system that depends on both position and velocity, it is relative degree 1. Similarly, with the goal of the robot tracking the human outputs, we consider the following actual and desired outputs:

$$y_{a,2}(\theta) = \begin{bmatrix} \delta m^R_{nsl}(\theta) \\ \theta_{sk} \\ \theta_{nsk} \\ \theta^R_{tor}(\theta) \end{bmatrix}, \; y_{d,2}(t) = \begin{bmatrix} m^d_{nsl}(t, \alpha_{nsl}) \\ \theta^d_{sk}(t, \alpha_{sk}) \\ \theta^d_{nsk}(t, \alpha_{nsk}) \\ \theta^d_{tor}(t, \alpha_{tor}) \end{bmatrix}, \tag{14}$$

where δm^R_{nsl} and θ^R_{tor} are the functions given in (2) and (3) computed with the parameters of the robot, and $y_{d,2}$ consists of the human walking functions given in (6). This is the first point in which it becomes apparent why we linearized the output functions describing the position of the hip and the non-stance leg slope; because of their linear form:

$$y_{a,2}(\theta) = H\theta \tag{15}$$

for $H \in \mathbb{R}^{4\times 5}$ with full row rank.

The goal is to drive the outputs to the outputs of the human as represented by the canonical walking functions, which motivates the final form of the outputs to be used in feedback linearization:

$$y_1(\theta, \dot\theta) = y_{a,1}(\theta, \dot\theta) - v_{hip}, \tag{16}$$

$$y_2(\theta) = y_{a,2}(\theta) - y_{d,2}(\tau(\theta)) \tag{17}$$

These outputs can be grouped together to form a single vector of *human-inspired outputs*:

$$y(\theta, \dot\theta) = \begin{bmatrix} y_1(\theta, \dot\theta) \\ y_2(\theta) \end{bmatrix} \tag{18}$$

where y_1 and y_2 will be seen to be relative degree 1 and vector relative degree 2 outputs, respectively. These outputs yield a *human-inspired controller*:

$$u(\theta, \dot\theta) = -\mathcal{A}^{-1}(\theta, \dot\theta)\left(\begin{bmatrix} 0 \\ L_{f_R} L_{f_R} y_2(\theta) \end{bmatrix} + \begin{bmatrix} L_{f_R} y_1(\theta, \dot\theta) \\ 2\varepsilon L_{f_R} y_2(\theta, \dot\theta) \end{bmatrix} + \begin{bmatrix} \varepsilon y_1(\theta, \dot\theta) \\ \varepsilon^2 y_2(\theta) \end{bmatrix}\right), \tag{19}$$

with control gain ε and decoupling matrix $\mathcal{A}(\theta)$ given by

$$\mathcal{A}(\theta, \dot\theta) = \begin{bmatrix} L_{g_R} y_1(\theta, \dot\theta) \\ L_{g_R} L_{f_R} y_2(\theta, \dot\theta) \end{bmatrix}$$

Note that the decoupling matrix is non-singular exactly because of the choice of output functions, i.e., as was discussed in Sect. 2, care was taken when defining the human outputs so that they were "mutually exclusive." It follows that for a control gain $\varepsilon > 0$, the control law u renders the output exponentially stable [16]. That is, the human-inspired output $y \to 0$ exponentially at a rate of ε; in other words, the outputs of the robot will converge to the canonical human walking functions exponentially.

Applying the feedback control law in (19) to the hybrid control system modeling the bipedal robot being considered, $\mathscr{HC}_R$ as given in (9), yields a hybrid system:

$$\mathscr{H}_R^{(\alpha,\varepsilon)} = (\mathcal{D}_R, S_R, \Delta_R, f_R^{(\alpha,\varepsilon)}), \tag{20}$$

where, $\mathcal{D}_R$, S_R, and Δ_R are defined as for $\mathscr{HC}_R$, and

$$f_R^{(\alpha,\varepsilon)}(\theta, \dot\theta) = f_R(\theta, \dot\theta) + g_R(\theta, \dot\theta)u(\theta, \dot\theta),$$

where the dependence of $f_R^{(\alpha,\varepsilon)}$ on the vector of parameters, α, and the control gain for the human-inspired controller, ε, has been made explicit.

5. HUMAN-INSPIRED PARTIAL HYBRID ZERO DYNAMICS

This section presents the main result of this paper through a culmination of the concepts presented thus far. Specifically, we present a method of obtaining parameters of the human-inspired controller (19) which provides the best fit of the human data, by minimizing (7), subject to constraints that guarantee that the resulting hybrid control system (20) has a stable periodic orbit. Furthermore, it is proven that a fixed point for this stable periodic orbit can be computed in closed form in the limit as $\varepsilon \to \infty$.

Hybrid Zero Dynamics (HZD). The human-inspired control law (19) drives the human-inspired outputs $y(\theta, \dot\theta) \to 0$

exponentially at a rate of ε. In particular, for the *continuous* dynamics of the hybrid system $\mathscr{H}_R^{(\alpha,\varepsilon)}$, the controller renders the *zero dynamics surface*:

$$\mathbf{Z}_\alpha = \{(\theta,\dot\theta) \in T\mathcal{Q}_R : y(\theta,\dot\theta) = \mathbf{0}_5,\ L_{f_R} y_2(\theta,\dot\theta) = \mathbf{0}_4\} \quad (21)$$

exponentially stable. Note that here $\mathbf{0}_p \in \mathbb{R}^p$ is a vector of zeros, and we make the dependence of $\mathbf{Z}_\alpha$ on the set of parameters explicit. It is at this point that continuous systems and hybrid systems diverge: while this surface is invariant for the continuous dynamics, it is not necessarily invariant for the hybrid dynamics. In particular, the discrete impacts in the system cause the state to be "thrown" off of the zero dynamics surface. Therefore, a hybrid system has *hybrid zero dynamics* if the zero dynamics are invariant through impact: $\Delta_R(S_R \cap \mathbf{Z}_\alpha) \subset \mathbf{Z}_\alpha$.

Partial Hybrid Zero Dynamics (PHZD). While the realization of HZD is the "best case scenario," it is quite difficult in the case of bipedal robotic walking since it would force the hybrid system to evolve on a 1-dimensional manifold. Therefore, we seek to enforce zero dynamics only for the relative degree 2 outputs. We refer to this as the *partial zero dynamics surface*, given by:

$$\mathbf{PZ}_\alpha = \{(\theta,\dot\theta) \in T\mathcal{Q}_R : y_2(\theta) = \mathbf{0}_4,\ \ L_{f_R} y_2(\theta,\dot\theta) = \mathbf{0}_4\} \quad (22)$$

The motivation for considering this surface is that it allows some "freedom" in the movement of the system to account for differences between the robot and human models. Moreover, since the only output that is not included in the partial zero dynamics surface is the output that forces the forward hip velocity to be constant, enforcing partial hybrid zero dynamics simply means that we allow the velocity of the hip to compensate for the shocks in the system due to impact.

Problem Statement. The goal of *human-inspired PHZD* is to find parameters α^* that solve the following constrained optimization problem:

$$\begin{aligned} \alpha^* = \underset{\alpha\in\mathbb{R}^{21}}{\operatorname{argmin}}\ & \mathrm{Cost}_{\mathrm{HD}}(\alpha) && (23)\\ \text{s.t}\quad & \Delta_R(S_R \cap \mathbf{Z}_\alpha) \subset \mathbf{PZ}_\alpha && \text{(PHZD)} \end{aligned}$$

with $\mathrm{Cost}_{\mathrm{HD}}$ the cost given in (7). This is simply the optimization problem in (8) that was used to determine the parameters of the canonical human walking functions that gave the best fit of the human walking functions to the human output data, but subject to constraints that ensure PHZD. The formal goal of this section is to restate (PHZD) in such a way that it can be practically solved.

Partial Zero Dynamics. This section utilizes the fact that the human outputs were specifically chosen to be linear in order to explicitly construct the *partial hybrid zero dynamics*. In particular, we reformulate the constructions in [22] in such a way as to be applicable to full-actuation (which is assumed in this case) and reframe them in the context of canonical human walking functions. Because of the specific choice of y_a in (14), we begin by picking the following representation of the partial zero dynamics:

$$\begin{aligned} \xi_1 &= \delta p^R_{\mathrm{hip}}(\theta) =: c\theta \\ \xi_2 &= y_{a,1}(\theta,\dot\theta) = \delta \dot p^R_{\mathrm{hip}}(\theta,\dot\theta) =: c\dot\theta \end{aligned} \quad (24)$$

where $c \in \mathbb{R}^{1\times 5}$ is obtained from (1). Moreover, since ξ_1 is just the linearized position of the hip, which was used to parameterize time (12), we can write $y_{d,2}(\tau(\theta)) = y_{d,2}(\xi_1)$. Picking the coordinates

$$\begin{aligned} \eta_1 &= y_a(\theta) = H\theta \\ \eta_2 &= L_{f_R} y_{a,2}(\theta,\dot\theta) = H\dot\theta \end{aligned} \quad (25)$$

with H as in (15), and defining

$$\begin{aligned} \Phi(\xi_1) &= \begin{bmatrix} c \\ H \end{bmatrix}^{-1} \begin{pmatrix} \xi_1 \\ y_{d,2}(\xi_1) \end{pmatrix} \\ \Psi(\xi_1) &= \begin{bmatrix} c \\ H \end{bmatrix}^{-1} \begin{pmatrix} 1 \\ \frac{\partial y_{d,2}(\xi_1)}{\partial \xi_1} \end{pmatrix} \end{aligned}$$

it follows that for $\theta = \Phi(\xi_1)$ and $\dot\theta = \Psi(\xi_1)\xi_2$, $(\theta,\dot\theta) \in \mathbf{PZ}_\alpha$.

As a result of the fact that we have full actuation and completely linearize the dynamics with (19), it follows that the relative degree 1 output evolves according to $\dot y_1 = -\varepsilon y_1$. Therefore, because of the definition of the partial zero dynamics, the partial hybrid zero dynamics evolve according to the linear ODE:

$$\begin{aligned} \dot\xi_1 &= \xi_2 \\ \dot\xi_2 &= -\varepsilon(\xi_2 - v_{\mathrm{hip}}). \end{aligned} \quad (26)$$

The advantage of the partial zero dynamics representation introduced is that it allows for the existence and stability of a fixed point of the zero dynamics to be determined *without integrating the ODE*. Specifically, given a point on the guard $(\theta^-,\dot\theta^-) \in S_R$ with its post-impact state $(\theta^+,\dot\theta^+) = \Delta_R(\theta^-,\dot\theta^-)$, we can compute $\xi_1^- = \delta p^R_{\mathrm{hip}}(\theta^-)$ and $\xi_1^+ = \delta p^R_{\mathrm{hip}}(\theta^+)$. From this, if (PHZD) is satisfied, the change in ξ_1 and ξ_2 due to this impact can be determined through:

$$\begin{aligned} \xi_1^+ &= \delta p^R_{\mathrm{hip}}(\Delta_\theta \theta^-) \\ \xi_2^+ &= \Delta_{\mathbf{PZ}}(\theta^-)\xi_2^- \end{aligned} \quad (27)$$

where θ^- is a point that is chosen *a priori* and

$$\Delta_{\mathbf{PZ}}(\theta^-) := c\Delta_{\dot\theta}(\theta^-)\Psi(\delta p^R_{\mathrm{hip}}(\theta^-)). \quad (28)$$

In essence, this defines a 2-dimensional hybrid system and therefore, when considering the existence and stability of a periodic orbit in the partial hybrid zero dynamics surface, one need only consider the restricted Poincaré map:

$$\rho : S_R \cap \mathbf{PZ}_\alpha \to S_R \cap \mathbf{PZ}_\alpha \quad (29)$$

where

$$S_R \cap \mathbf{PZ}_\alpha \cong \{(\xi_1,\xi_2) \in \mathbf{PZ}_\alpha :\ \xi_1 = \xi_1^-,\quad \xi_2 \in \mathbb{R}_{\geq 0}\}$$

In other words, the hyperplane $\xi_1 = \xi_1^-$ can be chosen as the Poincaré section. The Poincaré map for the partial hybrid zero dynamics is therefore a 1-dimensional (partial) map $\rho : S_R \cap \mathbf{PZ}_\alpha \to S_R \cap \mathbf{PZ}_\alpha$, and so ρ can be viewed as only a function of ξ_2 and therefore defines a discrete time dynamical system: $\xi_2[k+1] = \rho(\xi_2[k])$.

Inverse Kinematics. To achieve the goal of restating (23) in a way that is independent of state variables (position and velocity), we can use the outputs and guard functions to explicitly solve for the configuration of the system $\vartheta(\alpha) \in \mathcal{Q}_R$ on the guard $(h_R(\vartheta(\alpha)) = 0)$ in terms of the parameters α. In particular, let

$$\vartheta(\alpha) = \theta \quad \text{s.t} \quad \begin{bmatrix} y_2(\Delta_\theta\theta) \\ h_R(\theta) \end{bmatrix} = \begin{bmatrix} \mathbf{0}_4 \\ 0 \end{bmatrix}, \quad (30)$$

where Δ_θ is the relabeling matrix (11). Note that $\vartheta(\alpha)$ exists because of the specific structure of the outputs $y_2(\Delta_\theta\theta)$ chosen. In fact, the reason for considering y_2 at the point $\Delta_\theta\theta$ is because this implies that the configuration at the beginning of the step is $\theta^+ = \Delta_\theta\theta$ and thus $\tau(\Delta_\theta\theta) = 0$ implying that: $y_2(\Delta_\theta\theta) = H\Delta_\theta\theta - y_{d,2}(0)$, or (30) has a solution because of the simple form that y_2 takes at $\Delta_\theta\theta$.

Using $\vartheta(\alpha)$, we can explicitly solve for a point $(\vartheta(\alpha), \dot\vartheta(\alpha)) \in \mathbf{Z}_\alpha \cap S_R$. In particular, let

$$Y(\theta) = \begin{bmatrix} d\delta p^R_{\text{hip}}(\theta) \\ dy_2(\theta) \end{bmatrix}, \tag{31}$$

It follows from the definition of y_1 and y_2 that

$$\begin{bmatrix} y_1(\theta,\dot\theta) \\ L_{f_R} y_2(\theta,\dot\theta) \end{bmatrix} = Y(\theta)\dot\theta - \begin{bmatrix} v_{\text{hip}} \\ \mathbf{0}_4 \end{bmatrix}. \tag{32}$$

Therefore, define

$$\dot\vartheta(\alpha) = Y^{-1}(\vartheta(\alpha)) \begin{bmatrix} v_{\text{hip}} \\ \mathbf{0}_4 \end{bmatrix}, \tag{33}$$

where Y is invertible because of the choice of outputs.

Human-Inspired Optimization. With the notation of this section in hand, we define a *human-inspired optimization problem*; a proof of this theorem can be found in [3]. This constrained optimization uses the human data as a cost function (through the human-data-based cost (7)), but enforces constraints that, as is seen in the main result, ensure that the bipedal robot has a stable walking gait.

Theorem 1. The parameters α^* solving the constrained optimization problem:

$$\begin{aligned} \alpha^* = \underset{\alpha\in\mathbb{R}^{21}}{\text{argmin}}\ & \text{Cost}_{\text{HD}}(\alpha) && (34)\\ \text{s.t}\quad & y_2(\vartheta(\alpha)) = \mathbf{0}_4 && (\text{C1})\\ & dy_2(\Delta_\theta\vartheta(\alpha))\Delta_{\dot\theta}(\vartheta(\alpha))\dot\vartheta(\alpha) = \mathbf{0}_4 && (\text{C2})\\ & dh_R(\vartheta(\alpha))\dot\vartheta(\alpha) < 0 && (\text{C3}) \end{aligned}$$

yield partial hybrid zero dynamics: $\Delta_R(S_R \cap \mathbf{Z}_{\alpha^*}) \subset \mathbf{PZ}_{\alpha^*}$.

Main Result. The main result of this paper is that the point $(\vartheta(\alpha^*), \dot\vartheta(\alpha^*))$, determined through the inverse kinematics and utilizing the parameters obtained by solving the optimization problem in Theorem 1, is "essentially" the fixed point to a stable hybrid periodic orbit. Thus, the optimization problem in (34) not only ensures partial hybrid zero dynamics, but it automatically yields a fixed point to a stable walking gait that can be computed in closed form from the parameters of the human-inspired controller. Moreover, since the cost function (7) only depends on human walking data, we automatically generate a controller for a stable walking gait, its parameters, a stable hybrid periodic orbit and its fixed point using only human data.

Theorem 2. Let α^* be the parameters solving (34)*. If*

$$\tau(\vartheta(\alpha^*)) = \frac{\delta p^R_{\text{hip}}(\vartheta(\alpha^*)) - \delta p^R_{\text{hip}}(\Delta_\theta\vartheta(\alpha^*))}{v^*_{\text{hip}}} > 0$$

then there exists a constant $\bar\varepsilon > 0$ such that for all $\varepsilon > \bar\varepsilon$ the hybrid system $\mathscr{H}_R^{(\alpha^*,\varepsilon)}$ has an exponentially stable periodic orbit. Moreover, the fixed point of this periodic orbit, $(\theta^*_\varepsilon, \dot\theta^*_\varepsilon)$, is dependent on ε and satisfies the property that:

$$\lim_{\varepsilon\to\infty}(\theta^*_\varepsilon, \dot\theta^*_\varepsilon) = (\vartheta(\alpha^*), \dot\vartheta(\alpha^*)). \tag{35}$$

PROOF. From the proof of Theorem 1 in [3] it follows that $(\vartheta(\alpha^*), \dot\vartheta(\alpha^*)) \in \mathbf{Z}_\alpha \cap S_R$. Letting $\xi_1(\alpha^*)$ and $\xi_2(\alpha^*)$ be the representation of this point in the partial hybrid zero dynamics coordinates (24), the fact that $(\vartheta(\alpha^*), \dot\vartheta(\alpha^*)) \in \mathbf{Z}_\alpha$ implies that $\xi_2(\alpha^*) = v^*_{\text{hip}}$. By picking $\theta^- = \vartheta(\alpha^*)$ in (27), it follows that $\xi_1^- = \xi_1(\alpha^*)$. Due to the fact that the zero dynamics evolve in a linear fashion according to (26), the Poincaré map (29) can be explicitly computed; for $\xi_2 \in S_R \cap \mathbf{PZ}_\alpha$, it is given by

$$\rho_\varepsilon(\xi_2) = v^*_{\text{hip}}\left(1 + W\left(e^{-\varepsilon\tau(\vartheta(\alpha^*))}e^{\gamma(\xi_2)}\gamma(\xi_2)\right)\right)$$

where W is the Lambert W function (or product logarithm) and

$$\gamma(\xi_2) = \frac{\Delta_{\mathbf{PZ}}(\vartheta(\alpha^*))\xi_2 - v^*_{\text{hip}}}{v^*_{\text{hip}}}$$

determines the change in the (linearized) velocity of the hip relative to v^*_{hip}; or, in other words, the perturbation away from the zero dynamics surface $\mathbf{Z}_\alpha$. From the explicit form of the reduced Poincaré map ρ it follows that:

$$\lim_{\varepsilon\to\infty}\rho_\varepsilon(\xi_2) = v^*_{\text{hip}} = \xi_2(\alpha^*) \tag{36}$$

since $W(0) = 0$ and $\tau(\vartheta(\alpha^*)) > 0$.

To prove the existence of a periodic orbit for the partial hybrid zero dynamics, we need only prove the existence of a fixed point for ρ_ε. Consider a ball of radius $\delta > 0$ around v^*_{hip}, i.e., for $\xi_2 \in B_\delta(v^*_{\text{hip}})$, $|\xi_2 - v^*_{\text{hip}}| < \delta$. Then for this δ it follows by (36) that there exists a $\varepsilon_1 > 0$ such that for all $\varepsilon > \varepsilon_1$, $|\rho_\varepsilon(\xi_2) - v_{\text{hip}}| < \delta$. Therefore, $\rho_\varepsilon : B_\delta(v^*_{\text{hip}}) \to B_\delta(v^*_{\text{hip}})$. By the Brouwer fixed-point theorem, it follows that there exists a fixed point of ρ_ε, i.e., $\xi_2^*(\varepsilon)$, dependent on ε and satisfying $\rho_\varepsilon(\xi_2^*(\varepsilon)) = \xi_2^*(\varepsilon)$, and the hybrid partial zero dynamics has a periodic orbit. To prove the stability of this periodic orbit, we need only check the derivative of ρ_ε at $\xi_2^*(\varepsilon)$ and ensure that its magnitude is less than 1. The derivative ρ_ε can be explicitly computed as:

$$\rho'_\varepsilon(\xi_2^*(\varepsilon)) = \begin{cases} e^{-\varepsilon\tau(\vartheta(\alpha^*))}\Delta_{\mathbf{PZ}}(\vartheta(\alpha^*)) & \text{if} \quad \xi_2^*(\varepsilon) = v^*_{\text{hip}} \\ \frac{\Delta_{\mathbf{PZ}}(\vartheta(\alpha^*))^2(\xi_2^*(\varepsilon) - v^*_{\text{hip}})}{\Delta_{\mathbf{PZ}}(\vartheta(\alpha^*))\xi_2^*(\varepsilon) - v^*_{\text{hip}}} & \text{otherwise} \end{cases}$$

Since $\xi_2^*(\varepsilon) \to v^*_{\text{hip}} = \xi_2(\alpha^*)$ as $\varepsilon \to \infty$, it follows that

$$\lim_{\varepsilon\to\infty}\rho'_\varepsilon(\xi_2^*(\varepsilon)) = 0.$$

Therefore, there exists an $\varepsilon_2 > 0$ such that for $\varepsilon > \varepsilon_2$, $|\rho'_\varepsilon(\xi_2^*(\varepsilon))| < 1$ establishing the stability of the periodic orbit for the partial hybrid zero dynamics.

Finally, by Theorem 4.5 of [22] (see also [12]) a stable fixed point for the restricted Poincaré map ρ_ε implies that:

$$(\theta^*_\varepsilon, \dot\theta^*_\varepsilon) = (\Phi(\xi_1(\alpha^*)), \Psi(\xi_1(\alpha^*))\xi_2^*(\varepsilon)) \tag{37}$$

is a stable fixed point of the Poincaré map P_ε for the hybrid system $\mathscr{H}_R^{(\alpha^*,\varepsilon)}$ for ε sufficiently large, i.e., for $\varepsilon > \varepsilon_3$. Since (37) clearly satisfies (35), picking $\bar\varepsilon = \max\{\varepsilon_1, \varepsilon_2, \varepsilon_3\}$ implies the desired result. □

6. NAO IMPLEMENTATION

In this section, we show that the formal results of this paper can be used to achieve stable walking in a simulation of the NAO robot. Furthermore, by implementing the trajectories found in simulation, coupled with a lateral stability controller on the actual NAO robot (Fig. 4), we experimentally

achieve dynamically stable bipedal robotic walking; since the main purpose of this paper is the formal results, the discussion of the experimental results will necessarily be brief. We acknowledge that, as the formal results presented in this paper consider only the 2D sagittal dynamics of NAO, while the experimental implementation presented here is a good indication of successful control for complete validation of the theory, the 3D model with feet is required; this is a topic reserved for future work.

6.1 NAO Walking Simulation

We begin by discussing how the main results of this paper, Theorem 1 and 2, can be used to achieve walking in simulation for the 2D hybrid system model of NAO. These simulation results will serve as the basis for the control of the actual NAO robot.

Stable Robotic Walking. Beginning with the mean human output data, computed from the experimental human walking data and normalized with the NAO parameters, we apply the optimization in Theorem 1. To achieve practical results, additional constraints were enforced in this optimization which limited the maximum joint velocity to 3 rad/s and ensured proper foot clearance. This results in the parameters α^* for the human-inspired controller. As a result of Theorem 2, we automatically know that the parameters α^* will result in stable robotic walking for sufficiently large control gain ε. Picking $\varepsilon = 25$ and simulating the hybrid system $\mathscr{H}_R^{(\alpha^*,\varepsilon)}$ from the initial condition $(\vartheta(\alpha), \dot{\vartheta}(\alpha))$ verifies that we do, in fact, have a walking gait, i.e., a periodic orbit (see Fig. 5 and Fig. 6). Moreover, we can verify the fact that the chosen ε results in a stable walking gait by checking the eigenvalues of the Poincaré map; we find that the magnitude of the maximum eigenvalue is $\lambda = 0.1059$, thus verifying the exponential stability guaranteed by Theorem 2. Furthermore, and as indicated in Fig. 5, the resulting walking exhibits partial hybrid zero dynamics. Finally, we computed the specific cost of transport (SCOT) for this walking to be 0.33 which, given the differences between NAO and a human, is reasonably close to the human value of 0.20 (see [6]). It is important to note that, since the simulated model only has point feet (which was used to approximate the fact that the feet are assumed to always be flat during the walking on the actual NAO robot), the walking obtained in simulation is necessarily dynamically stable.

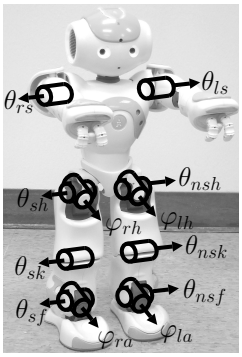

Figure 4: Angle conventions for NAO with right foot as stance foot.

Walking from Rest. In addition to stable, periodic walking, the robustness of the human-inspired control law allows for the robot to start from rest and converge to the walking periodic orbit corresponding to the walking gait. As shown in Fig. 5, trajectories of the system when started from rest converge to the stable limit periodic orbit predicted by Theorem 2. Convergence is also seen in a plot of the human inspired outputs; in Fig. 5 the convergence of the actual outputs of the robot to the desired outputs can be seen. Tiles of the first step of the walking, starting from rest, can be seen in Fig. 6. As discussed in the following section, the trajectories of the simulated NAO model, starting from rest, can be used to experimentally achieve walking in the real NAO robot.

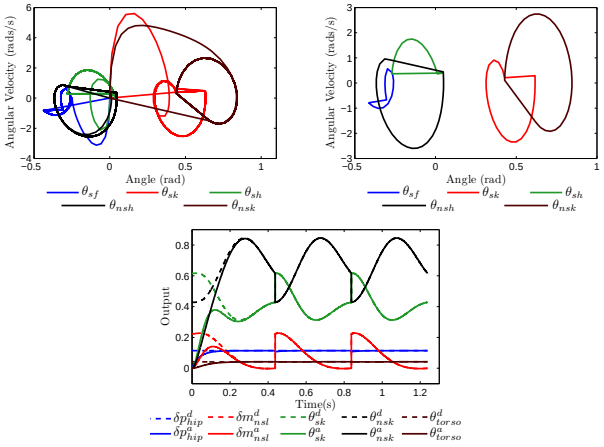

Figure 5: Periodic orbits for the simulated behavior of NAO starting from rest, i.e., a zero initial condition (top left) and the fixed point of the periodic orbit (top right). Starting from rest, the actual outputs of NAO converge to the desired outputs and display partial hybrid zero dynamics (bottom).

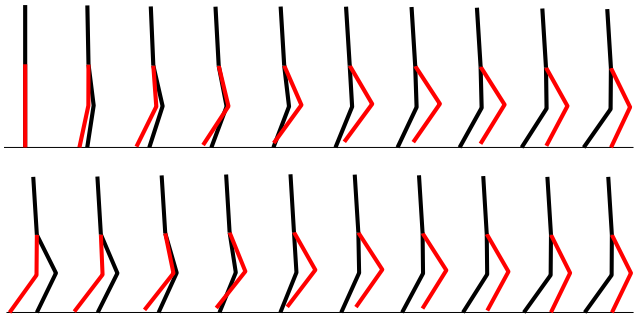

Figure 6: Snapshots of the walking gaits from the NAO simulation starting from zero initial conditions (top) and starting from the fixed point $(\vartheta(\alpha), \dot{\vartheta}(\alpha))$ (bottom).

6.2 NAO Walking Experiment

The end goal of the human-inspired walking control design process is the realization of stable walking on an actual robot. Aldebaran's NAO robot was chosen for implementation of the ideas presented in this paper; therefore, we use it as a testbed to show experimental validation of the formal results for the 2D model of the NAO presented in this paper and, more generally, the framework of human-inspired control.

Implementation. To implement the simulated walking behavior on NAO, we use trajectory tracking of the simulated behavior for the sagittal angles and design and implement a lateral stability controller to maintain lateral balance through the walking gait. Specifically, stance and swing joint

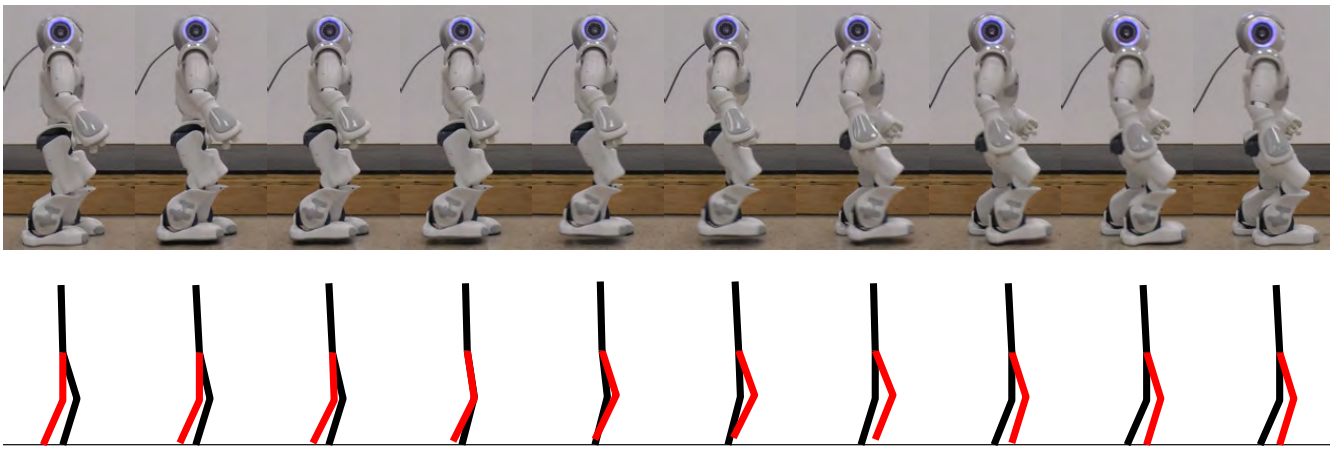

Figure 7: Comparison of the snapshots of the actual (top) and simulated (bottom) walking gaits over one step.

angle trajectories are taken from the simulated behavior of the robot. The control software then takes these individual steps and compiles them into joint trajectories for sagittal angles of the left and right legs (essentially "undoing" the simplifying assumption of a "stance" and "non-stance" leg used in the modeling of the robot). To help maintain lateral stability during walking, we implement a simple online feedback controller with the objective of driving the absolute vertical roll-angle of the NAO's chest to zero in order to decrease lateral instability. In particular, we measure the absolute angle of NAO's chest, φ^a_{chest}, through the onboard IMU. The desired lateral angles of NAO are then defined as $\varphi^d_{lh} = \varphi^d_{rh} = K_{hip}\varphi^a_{chest}$ and $\varphi^d_{la} = \varphi^d_{ra} = -K_{ankle}\varphi^a_{chest}$, with $K_{hip} = 0.7$ and $K_{ankle} = 0.77$, which NAO then tracks with the onboard joint angle controllers.

Results. Implementing the simulated trajectories of the human-inspired walking control on NAO results in dynamically stable walking on the *actual* NAO robot. Tiles of the walking gait achieved in experimentation can be seen in Fig. 7; in that figure, the experimental walking is compared against tiles of the simulated walking taken at the same time instances showing that, in fact, there is good agreement. To provide qualitative evidence of this, the simulated and experimentally observed figures are plotted in Fig. 8; this shows excellent agreement between simulation and experimentation. In this same figure, the effects of the lateral stability controller are shown; the lateral angles oscillate to provide stability in the lateral plane. To verify that the walking obtained on NAO is dynamically stable, we compute the position of the center of mass from the experimental data and check to ensure that it is not over the foot during the course of the walking. Due to the size of the feet on NAO, we find that the y-position of the center of mass is more revealing; as shown in Fig. 9, the center of mass is almost never over the feet during the walking gait. Thus we conclude that the robotic walking achieved is dynamically stable. Finally, the human-inspired walking that was obtained on NAO subjectively appears more human-like that other walking gaits that have been achieved for NAO. We invite readers to form their own opinions by watching the video of the human-inspired robotic walking, and its comparison with the pre-existing (ZMP) walking, which is available online [2].

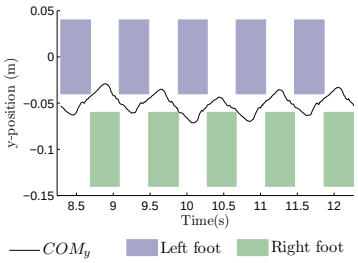

Figure 9: The y-position of the center of mass over multiple steps, with the width of the left and right foot indicated. Since the position of the center of mass is not over either the left or right foot, the experimental walking obtained is dynamically stable.

7. CONCLUSIONS

This paper presents a formal, human-inspired approach to bipedal robotic walking, proving through Theorem 1 and 2 that, by using only human data, parameters to the human-inspired controller can be determined that simultaneously: provide the best fit of the human data, yield partial hybrid zero dynamics, imply the existence of a stable walking gait, and allow the fixed point for this stable walking gait to be explicitly computed. As a result, this method allows for the rapid generation of stable walking gaits during the controller development for bipedal robotic walking simulations and experiments, such as those performed on Aldebaran's NAO robot in this paper. Future work on this topic includes expansion of the formal results to the 3D model of NAO and examination of the accompanying constraints, such as ZMP and friction.

Acknowledgments

The work of A. D. Ames is supported by NSF grant CNS-0953823 and NHARP award 00512-0184-2009. The work of M. J. Powell is supported by NASA grant NNX11AN06H.

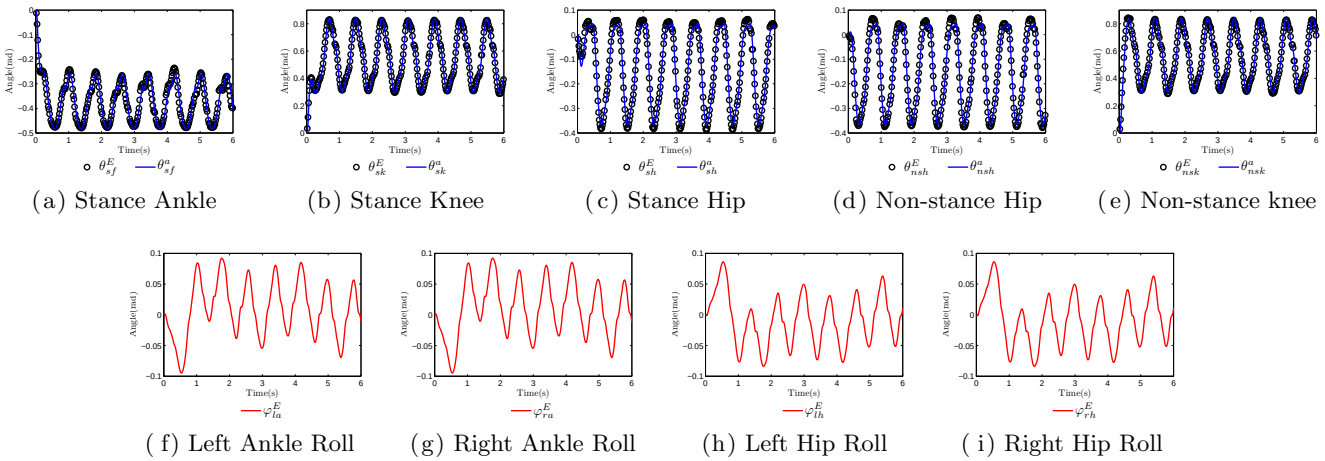

(a) Stance Ankle (b) Stance Knee (c) Stance Hip (d) Non-stance Hip (e) Non-stance knee

(f) Left Ankle Roll (g) Right Ankle Roll (h) Left Hip Roll (i) Right Hip Roll

Figure 8: Simulated (desired) and experimental joint trajectories for the sagittal plane (a)-(e), and angles in the lateral plane controlled through the lateral stability controller (f)-(i) as seen in experimentation (see Fig. 4 for the angle conventions).

8. REFERENCES

[1] `http://www.aldebaran-robotics.com/`.

[2] `http://www.youtube.com/watch?v=OBGHU-e1kc0/`.

[3] A. D. Ames. First steps toward automatically generating bipedal robotic walking from human data. In *8th International Workshop on Robotic Motion and Control, RoMoCo'11*, Bukowy Dworek, Poland, 2011.

[4] A. D. Ames and R. D. Gregg. Stably extending two-dimensional bipedal walking to three dimensions. In *26th American Control Conference*, New York, NY, 2007.

[5] A. D. Ames, R. Vasudevan, and R. Bajcsy. Human-data based cost of bipedal robotic walking. In *Hybrid Systems: Computation and Control*, Chicago, IL, 2011.

[6] S. Collins and A. Ruina. A bipedal walking robot with efficient and human-like gait. In *International Conference on Robotics and Automation*, Barcelona, Spain, 2005.

[7] J. W. Grizzle, G. Abba, and F. Plestan. Asymptotically stable walking for biped robots: Analysis via systems with impulse effects. *IEEE TAC*, 46(1):51–64, 2001.

[8] J. W. Grizzle, C. Chevallereau, A. D. Ames, and R. W. Sinnet. 3D bipedal robotic walking: models, feedback control, and open problems. In *IFAC Symposium on Nonlinear Control Systems*, Bologna, Italy, 2010.

[9] P. Holmes, R. Full, D. Koditschek, and J. Guckenheimer. The dynamics of legged locomotion: Models, analyses, and challenges. *SIAM Review*, 48:207–304, 2006.

[10] Y. Hürmüzlü and D. B. Marghitu. Rigid body collions of planar kinematic chains with multiple contact points. *Intl. J. of Robotics Research*, 13(1):82–92, 1994.

[11] S. Kajita, F. Kanehiro, K. Kaneko, K. Fujiwara, K. Harada, K. Yokoi, and H. Hirukawa. Biped walking pattern generator allowing auxiliary ZMP control. In *IEEE/RSJ Intl. Conf. on Intelligent Robots and Systems*, pages 2993–2999, Beijing, P.R. China, 2006.

[12] B. Morris and J. Grizzle. A restricted Poincaré map for determining exponentially stable periodic orbits in systems with impulse effects: Application to bipedal robots. In *IEEE Conf. on Decision and Control*, Seville, Spain, 2005.

[13] R. M. Murray, Z. Li, and S. S. Sastry. *A Mathematical Introduction to Robotic Manipulation*. CRC Press, Boca Raton, 1994.

[14] J. Pratt, J. Carff, and S. Drakunov. Capture point: A step toward humanoid push recovery. In *in 6th IEEE-RAS International Conference on Humanoid Robots*, Genoa, Italy, 2006.

[15] J. Rose and J. G. Gamble. *Human Walking*. Lippincott Williams & Wilkins, Philadelphia, 2005.

[16] S. S. Sastry. *Nonlinear Systems: Analysis, Stability and Control*. Springer, New York, 1999.

[17] R. W. Sinnet and A. D. Ames. 3D bipedal walking with knees and feet: A hybrid geometric approach. In *48th IEEE Conference on Decision and Control*, Shanghai, P.R. China, 2009.

[18] M. W. Spong and F. Bullo. Controlled symmetries and passive walking. *IEEE TAC*, 50(7):1025–1031, 2005.

[19] S. Srinivasan, I. A. Raptis, and E. R. Westervelt. Low-dimensional sagittal plane model of normal human walking. *ASME J. of Biomechanical Eng.*, 130(5), 2008.

[20] M. Vukobratović and B. Borovac. Zero-moment point—thirty-five years of its life. *Intl. J. of Humanoid Robotics*, 1(1):157–173, 2005.

[21] E. Wendel and A. D. Ames. Rank properties of Poincaré maps for hybrid systems with applications to bipedal walking. In *Hybrid Systems: Computation and Control*, Stockholm, Sweden, 2010.

[22] E. R. Westervelt, J. W. Grizzle, C. Chevallereau, J. H. Choi, and B. Morris. *Feedback Control of Dynamic Bipedal Robot Locomotion*. CRC Press, Boca Raton, 2007.

[23] E. R. Westervelt, J. W. Grizzle, and D. E. Koditschek. Hybrid zero dynamics of planar biped walkers. *IEEE TAC*, 48(1):42–56, 2003.